Stacking faults and metallic properties of triangular lattice CoO_2 with a three-layer structure

2008 J. Phys.: Condens. Matter 20 175207

(http://iopscience.iop.org/0953-8984/20/17/175207)

J. Phys.: Condens. Matter **20** (2008) 175207 (6pp) doi:10.1088/0953-8984/20/17/175207

Stacking faults and metallic properties of triangular lattice CoO_2 with a three-layer structure

Masashige Onoda and Asami Sugawara

Institute of Physics, University of Tsukuba, Tennodai, Tsukuba 305-8571, Japan

E-mail: onoda@sakura.cc.tsukuba.ac.jp

Received 1 November 2007, in final form 22 February 2008
Published 3 April 2008
Online at stacks.iop.org/JPhysCM/20/175207

Abstract

A triangular lattice system CoO_2 is synthesized through chemical extraction of Li from $LiCoO_2$ with H_2SO_4. On the basis of the x-ray powder diffraction and various composition analyses, the structure approximately modelled with space group $R\bar{3}m$ and cell dimensions $a = 2.8388(6)$ and $c = 13.439(1)$ Å in the hexagonal basis has three oxygen layers with a prismatic oxygen environment (P3) between the layers. It also has stacking faults with shift vectors $\boldsymbol{s}_1 = \frac{2}{3}\boldsymbol{a} + \frac{1}{3}\boldsymbol{b}$ and $\boldsymbol{s}_2 = \frac{1}{3}\boldsymbol{a} + \frac{2}{3}\boldsymbol{b}$ along the shift of $\frac{1}{3}\boldsymbol{c}$. Through measurements of the thermoelectric power and magnetic susceptibility, CoO_2 (P3) is suggested to be a weakly correlated metal with a mass enhancement of 2.6. $Na_{0.09}CoO_2$ synthesized through Na extraction from $Na_{0.7}CoO_2$ also shows metallic properties with correlation effects probably stronger than those of CoO_2 (P3).

1. Introduction

Transition-metal oxides and the nonstoichiometric bronzes have aroused considerable interest from both the basic science and applied viewpoints. For example, many oxides with partially filled d orbitals, which contain high-T_c superconductors and related compounds, have been investigated to clarify the properties of correlated electron systems and quantum spin-fluctuation systems [1]. They are also utilized as various functional materials such as thermoelectric devices [2, 3] or rechargeable lithium batteries [3]. These basic and applied properties are essentially related to the structures formed by the linkage of rigid units such as the TO_6 octahedra or TO_4 tetrahedra, where T is a transition-metal atom.

The triangular lattice system Co oxides have several remarkable characteristics such as superconductivity in $Na_{0.3}CoO_2{\cdot}1.3H_2O$ [4] and the possible application to thermoelectric devices in Na_xCoO_2 [2]. In the Na_xCoO_2 system that has several different phases with sheets of edge-sharing CoO_6 octahedra interleaved by Na [5], special attention has been paid to the γ phase [6]. This phase has a two-layer triangular lattice structure, where the Na atoms are located in a trigonal prismatic environment and they are partially occupied. Thus, the γ phase is expressed as 'P2'. The phase diagram as a function of the Na concentration [7] indicates that, as x increases from ≈0.3 to ≈0.8, the ground state goes from a normal metal to a Curie–Weiss metal through a poor metallic state at $x \approx 0.5$ accompanied by a partial valence order of Co [6]. Recently, a new type of triangular lattice $H_{0.3}CoO_2$ prepared with soft-chemistry synthesis was found to have a P2 structure and to exhibit weakly correlated or normal metallic properties [8].

The Li_xCoO_2 system is a well-known triangular lattice oxide, being used in Li rechargeable batteries [9]. The structure for $x = 1$ is α-$NaFeO_2$ type with octahedral coordination for alkali atoms and the three layers of oxygens, which are called 'O3'. The structural aspects and the metal–insulator transitions in the Li de-intercalated process have been studied, especially relating to the performance of the battery.

CoO_2 is the $x = 0$ end-member compound for Na_xCoO_2 and Li_xCoO_2. The compound prepared with an electrochemical de-intercalation of Li for $LiCoO_2$ has a CdI_2-type 'O1' structure with space group $P\bar{3}m1$ and cell dimensions of $a = 2.822$ and $c = 4.293$ Å [10]. On the other hand, a soft-chemical synthesis with NO_2BF_4 provides a 'P3' structure, where the space group is noncentrosymmetric $R3m$ and cell dimensions are $a = 2.833$ and $c = 13.496$ Å [11]. Hereafter, the CoO_2 compounds with O1 and P3 structures are referred to as CoO_2 (O1) and CoO_2 (P3), respectively. A recent nuclear magnetic resonance (NMR) study for CoO_2 (O1) reveals a metallic ground state [12].

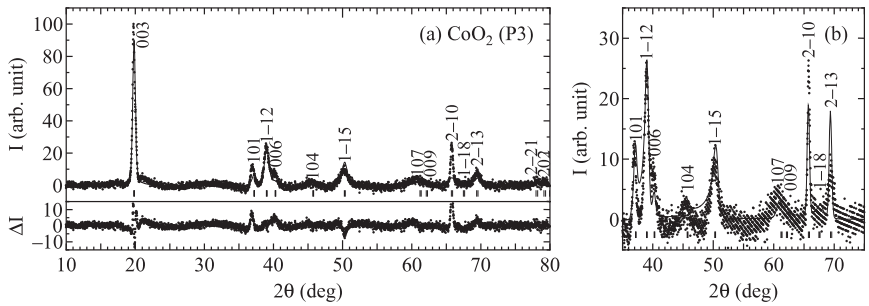

Figure 1. (a) The overall x-ray powder diffraction pattern and (b) its magnified drawing of CoO_2 (P3) with Cu Kα radiation at 293 K. Here, the full curves in the top panel of (a) and (b) indicate the results in terms of Rietveld refinement and the simulation on stacking faults, respectively, and the bottom panel of (a) denotes the differences between the observed and calculated intensities for the refinement.

This paper considers CoO_2 (P3) derived from the nominal compound $LiCoO_2$ with soft-chemistry synthesis. In addition, the properties of $Na_{0.09}CoO_2$ prepared from $Na_{0.7}CoO_2$ are described. Details regarding the sample preparation and the measurements are given in section 2. The structural model of CoO_2 (P3) constructed with x-ray powder diffraction and various composition analyses is presented in section 3.1; the transport properties revealed through measurements of the electrical resistivity and thermoelectric power are described in section 3.2, and magnetic properties for the susceptibility and electron spin resonance (ESR) are given in section 3.3. Section 4 is devoted to conclusions.

2. Experiments

Polycrystalline specimens of CoO_2 (P3) were synthesized by the soft-chemistry method as follows. First, nominal compounds of $LiCoO_2$ were made with the solid-state reaction from a mixture of $3Li_2CO_3$ and $2Co_3O_4$ at 1033 K in air. The compounds obtained here ($\sim 1.5 \times 10^{-3}$ kg) were stirred in 0.3 l of H_2SO_4 with 10 mol l^{-1} for 6 days in air. The polycrystalline specimens of $Na_{0.09}CoO_2$ were prepared by stirring about 10^{-3} kg of $Na_{0.7}CoO_2$ prepared following the procedure in [13] in 0.3 l of H_2SO_4 with 9.4 mol l^{-1} for 2 days in air. For both of the compounds, H_2SO_4 was repurified every other day. By washing them with water and drying in air, the powder specimens were finally obtained. For measurements of the physical properties described below, the specimens were pressed into pellets at a pressure of 2.5×10^7 N m^{-2}, which led to packing factors between 70 and 85%.

An inductively coupled plasma-optical emission spectroscopy (ICP) was done using a Nippon Jarrell-Ash ICAP-575 spectrometer. A thermogravimetric analysis (TG) for the CoO_2 (P3) specimen was carried out at temperatures between 300 and 923 K in Ar atmosphere using an SII EXSTAR6000 TG/DTA. In order to check whether the CoO_2 (P3) specimen contains H atoms or not, the magic-angle spinning (MAS) NMR spectra were taken with spinning speeds of 10 kHz using a Bruker Avance spectrometer under 14 T at 293 K. An x-ray powder diffraction pattern was taken with Cu Kα radiation at 293 K using a Rigaku RAD-IIC diffractometer. The four-terminal electrical resistivity and the thermoelectric power were measured with the dc method at temperatures between 4.2 and 300 K. The magnetization measurements were performed at temperatures between 4.2 and 300 K by the Faraday method with a field of up to 1 T. The magnetic susceptibility was deduced from the linear part of the magnetization–field curve with a decreasing field. The ESR spectra for $Na_{0.09}CoO_2$ were taken at 9.2 GHz using a JEOL TE200 spectrometer at temperatures between 5 and 300 K.

3. Results and discussion

3.1. Structural model

On the basis of ICP analysis, the specimens prepared from $LiCoO_2$ and $Na_{0.7}CoO_2$ are determined to have compositions of CoO_2 and $Na_{0.09}CoO_2$, respectively. For the CoO_2 specimen, Li ions of 0.01 per Co are detected, but this is considered to come from an impurity adhered to the surface as will be supported with the structure analysis. The MAS NMR analysis shows the absence of H atoms and the TG analysis indicates an oxygen concentration per Co of 1.98 through the reduction to Co_3O_4, which is close to the stoichiometric value.

Figure 1 indicates the x-ray powder diffraction pattern for the CoO_2 (P3) specimen at 293 K. The diffraction peaks are indexed as a trigonal cell with hexagonal axis dimensions $a = 2.8388(6)$ and $c = 13.439(1)$ Å, comparable with the previous report prepared with NO_2BF_4 [11]. The initial phase of structure was determined by direct methods [14] with the assumption of centrosymmetric space group $R\bar{3}m$. On the basis of the Rietveld analysis [15], the structure is approximately modelled with zero thermal factors, as listed in table 1, and corresponds to the 'P3' structure. Here, the discrepancy factors are $R_p = \sum |Y_o - Y_c| / \sum |Y_o| = 7.1$ % and $R_{wp} = [\sum w(Y_o - Y_c)^2 / \sum w Y_o^2]^{1/2} = 9.6\%$, where Y_o and Y_c are the observed and calculated intensities of the pattern, respectively. The alkali-metal extraction for $Na_{0.3}CoO_2$ with H_2SO_4 provides the compound $H_{0.3}CoO_2$ [8], but this is not the case, since the MAS NMR reveals the absence of H, and the nearest neighbour O–O distance between the layers (2.761(16) Å) is too large to put the two-coordinated H atom in the middle of this bond [16]. The clinographic view of the structural model of CoO_2 (P3) is shown in figure 2(a). For comparison, the structure of $LiCoO_2$ (O3) made for the soft-chemical preparation of CoO_2 (P3), which is refined by referring to the atomic parameters for unmodulated crystals

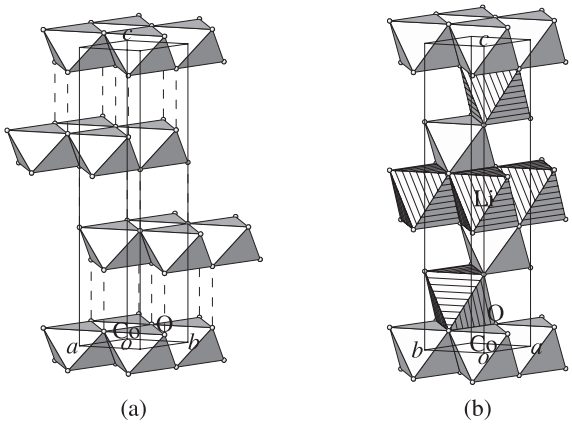

Figure 2. The clinographic views for the structural models of (a) CoO_2 (P3) and (b) $LiCoO_2$ (O3) with the polyhedral scheme.

Table 1. Atomic coordinates of CoO_2 (P3) modelled with zero thermal factors at 293 K.

Atom	Site	Occupancy	x	y	z
Co	3a	1	0	0	0
O	6c	1	$\frac{1}{3}$	$\frac{2}{3}$	0.0639(9)

of $LiVO_2$ in the paramagnetic state [17], is indicated in figure 2(b), where the space group is $R\bar{3}m$ and cell dimensions are $a = 2.8147(1)$ and $c = 14.0470(9)$ Å, consistent with the published data [9].

The Co ions are surrounded octahedrally with a Co–O distance of 1.850(5) Å. As shown in figure 2(a), there exist three triangular lattice layers of CoO_2 linked by edge-shared CoO_6 octahedra in the unit cell. This stacking gives rise to the factor of 3 increase in the c-axis compared with the CoO_2 (O1) unit. Strictly speaking, the $c/3$ value of 4.480 Å is larger than the fundamental unit for CoO_2 (O1) [10], which may be attributed to the Coulomb interaction between the oxygen layers as described below. On the basis of the bond-lengths–bond-strength relation [18], the effective valence of Co is estimated to be 4.0, which agrees well with that from the chemical formula assuming the full occupancy of O ions.

The diffraction pattern is roughly explained with the above structural model. Here, it should be noted that reflections with a condition of $h - k = 3n$, n being an integer, remain sharp compared with other peaks, as shown in figure 1(b). This may be a characteristic of the stacking faults for the c-direction. In order to simulate this effect, the profile is simulated in terms of a DIFFaX program [19].

A two-dimensional array of edge-shared CoO_6 octahedra defined as L_1 or one kind of fundamental layer unit expressed by Co in (0 0 0) and O in $\pm(\frac{1}{3}\ \frac{2}{3}\ 0.0639)$ is considered. The remaining two layers of L_2 and L_3 are obtained from L_1 by the shift vectors of $\boldsymbol{s}_1 = \frac{2}{3}\boldsymbol{a} + \frac{1}{3}\boldsymbol{b}$ and $\boldsymbol{s}_2 = \frac{1}{3}\boldsymbol{a} + \frac{2}{3}\boldsymbol{b}$, respectively, along the shift of $\frac{1}{3}\boldsymbol{c}$. In order to maintain the structure shown in figure 2(a), each layer unit (L_1, L_2 or L_3) can be followed by one of L_1, L_2 and L_3. Considering the Coulomb interaction between the layers, the sequence in which the neighbouring layer units are the same does not occur. Thus, the model of stacking faults, in which the stackings by $\boldsymbol{s}_1$ and $\boldsymbol{s}_2$ occur with the probabilities of $1 - \alpha$ and $1 - \alpha'$, respectively, is adopted. The full curve in figure 2(b) is the result calculated for $\alpha = 0.1$ and $\alpha' = 0.25$, which successfully explains the profile. The reason why such stacking faults exist in CoO_2 (P3) may be that the Coulomb repulsion between the oxygen layers increases without doping guest atoms.

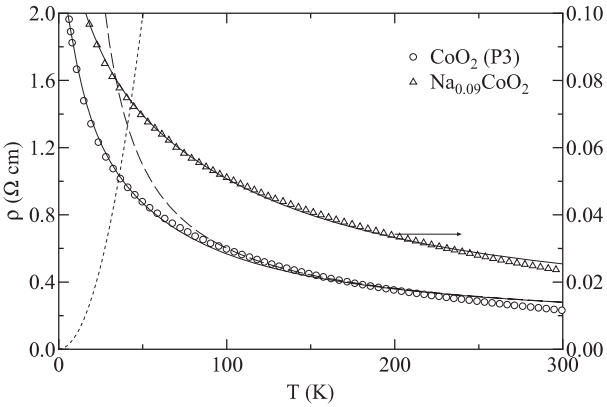

Figure 3. The temperature dependences of the electrical resistivities for CoO_2 (P3) and $Na_{0.09}CoO_2$, where the full curves denote fits to equation (1) with parameters listed in table 2. The dotted and dashed curves for CoO_2 (P3) indicate the behaviours of $\rho_m - \rho_0$ and ρ_v, respectively.

For $Na_{0.09}CoO_2$, the diffraction profile has large peak widths, indicating a poor crystallinity and/or heavy stacking faults. Since relatively weak reflections are not clear, only cell dimensions for the fundamental layer unit in a hexagonal basis are determined as $a = 2.821(1)$ and $c = 4.860(7)$ Å.

3.2. Transport properties

The temperature dependences of the electrical resistivities ρ for CoO_2 (P3) and $Na_{0.09}CoO_2$ are shown in figure 3. The result that the resistivity appears to exhibit nonmetallic behaviours may be attributed to intergrain conductions as in the case of $H_{0.3}CoO_2$ [8]. Considering a parallel combination of the metallic resistivity (ρ_m) with a power of p and the variable-range hopping (VRH) resistivity in three dimensions (ρ_v) for the loosely packed specimen [20] expressed as

$$\rho^{-1} = \rho_m^{-1} + \rho_v^{-1} = (\rho_0 + AT^p)^{-1} + B^{-1}\exp[(T_0/T)^{-1/4}], \quad (1)$$

where ρ_0 is the residual resistivity, the data are almost fitted with the parameters listed in table 2, as shown in figure 3 by the full curves. The dotted and dashed curves for CoO_2 (P3) in this figure represent the behaviours of $\rho_m - \rho_0$ and ρ_v, respectively. Here, the VRH parameters are mainly due to an extrinsic origin, so that the consideration is not necessary. The metallic resistivity is suggested to follow the Fermi-liquid relation as far as this model is assumed, although the values of ρ_0 and A much larger than those near the metal–insulator boundary for the perovskite system [21, 22] may be attributed to the loose packing of the specimen as well as the correlation effect.

The thermoelectric power S should reflect more intrinsic properties, since it is not significantly influenced by the

Table 2. The parameters of transport properties for CoO_2 (P3) and $Na_{0.09}CoO_2$.

	ρ_0 (Ω cm)	A (mΩ cm K^{-2})	p	B (mΩ cm)	T_0 (10^4 K)	E_F ($10^3 q$ K)
CoO_2 (P3)#1	2.22(1)	0.79(11)	2	25.1(9)	1.01(5)	6.9
CoO_2 (P3)#2	—	—	—	—	—	6.0
$Na_{0.09}CoO_2$	0.1195(5)	0.015(1)	2	1.59(4)	1.80(7)	8.1

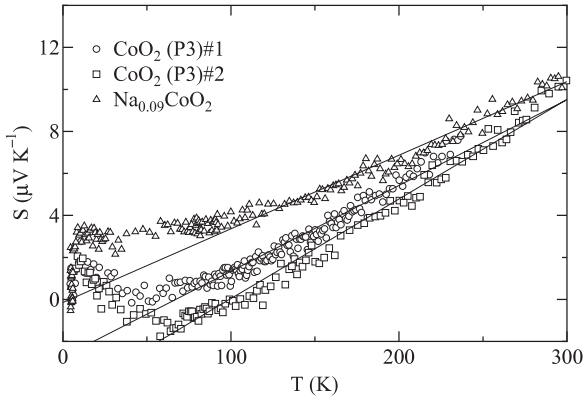

Figure 4. The temperature dependences of the thermoelectric powers for CoO_2 (P3) and $Na_{0.09}CoO_2$, where the full lines denote fits to equation (2) with parameters given in table 2.

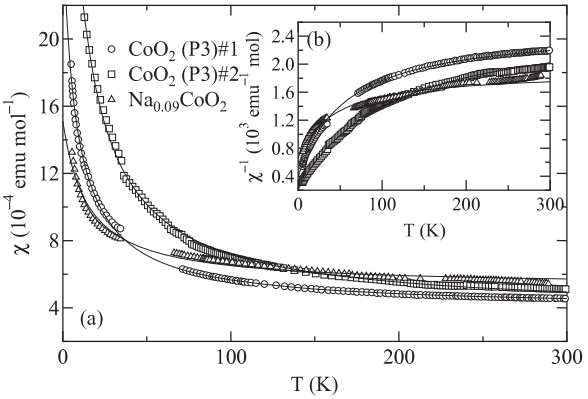

Figure 5. The temperature dependences of (a) the magnetic susceptibilities and (b) their inverses for CoO_2 (P3) and $Na_{0.09}CoO_2$, where the full curves in (a) and (b) denote fits to equation (3) with parameters given in table 3.

intergrain transport. The temperature variations of the thermoelectric powers for CoO_2 (P3) and $Na_{0.09}CoO_2$ are shown in figure 4. For both of the compounds, the thermoelectric powers are positive except for the small part at low temperatures for CoO_2 (P3), indicating the carrier to be essentially hole. The thermoelectric power for CoO_2 (P3) has a dependence linear in temperature above 50 K, below which it is nearly zero. For $Na_{0.09}CoO_2$, it is linear in temperature above 100 K, below which it is constant, about 3 μV K^{-1} down to 7 K, and then it nearly goes to zero. These temperature dependences and the magnitudes smaller than 10 μV K^{-1} suggest that both of the compounds are metallic, although the overall behaviours are different from that expected from Fermi-liquid theory. Applying the relation

$$S = \frac{\pi^2 k^2 T}{3e} \frac{\mathrm{d} \ln \sigma(E)}{\mathrm{d}E}\bigg|_{E_F}, \qquad (2)$$

where k is the Boltzmann constant, $\sigma(E)$ is a conductivity-like function of electron energy E with the form $\sigma(E) \propto E^q$, and E_F is the Fermi energy, to the data at high temperatures, E_F values for CoO_2 (P3) #1 (#2) and $Na_{0.09}CoO_2$ are estimated as listed in table 2 on the basis of the full lines in figure 4. The exponent q may be estimated with E_F obtained from another experiment. Considering that the parallel combination model of ρ_m and ρ_v would be effective for this case, the thermoelectric power is given with a conductivity-weighted mean of S_m and S_v, where $S_{m(v)}$ is the thermoelectric power from the path related to $\rho_{m(v)}$. However, this model is too simplified to explain the data, since it corresponds to a limit for the two kinds of transport paths. On the other hand, due to the particle–hole symmetry, the one-dimensional Hubbard model with a half-filled band should lead to zero thermoelectric power for general finite Coulomb repulsion energy [23], which would also be consistent with the small value of S at low temperatures for CoO_2 (P3). However, it may not be the case, since $Na_{0.09}CoO_2$ with a CoO_2 plane similar to that of CoO_2 (P3) also exhibits a small value in spite of the carrier concentration $n \neq 1$.

3.3. Magnetic properties

The magnetic susceptibilities χ and their inverses of CoO_2 (P3) and $Na_{0.09}CoO_2$ as a function of temperature are shown in figures 5(a) and (b), respectively. Here the data containing the contribution from the slightly adsorbed oxygens are removed. The temperature dependence is apparently expressed as

$$\chi = C/(T + T_W) + \chi_0, \qquad (3)$$

where the first term is the Curie–Weiss susceptibility χ_{CW} with the Curie constant C and the Weiss temperature T_W, and the second term is the temperature-independent component from the orbital susceptibility χ_{orb}, diamagnetic susceptibility χ_{dia}, and so on. Fits to equation (3) provide the parameters listed in table 3. Since the Curie constants obtained for CoO_2 (P3) #1 and $Na_{0.09}CoO_2$ are smaller than 4% of the value for $S = \frac{1}{2}$ and $g = 2$, the temperature-dependent contributions may be attributed to impurities and/or lattice imperfections. This is supported by a preliminary NMR result of the ^{59}Co nuclei in CoO_2 (P3) which indicates that the Knight shift is nearly temperature independent between 5 and 50 K, since this measurement reflects the major part of specimens and is not sensitive to the impurity [24].

The constant components χ_0 are one order of magnitude larger than those of usual simple metals [25], suggesting the correlated nature of the electrons. Since the transport

Table 3. The parameters of magnetic properties for CoO_2 (P3) and $Na_{0.09}CoO_2$.

	C (emu K mol^{-1})	T_W (K)	χ_0 (emu mol^{-1})
CoO_2 (P3)#1	0.0185(2)	8.5(1)	3.95(1)
CoO_2 (P3)#2	0.0374(3)	8.3(1)	3.73(2)
$Na_{0.09}CoO_2$	0.0142(6)	14.5(1)	5.26(4)

properties for both of the compounds are essentially metallic, an enhanced Pauli susceptibility, $\chi_P = \mu_B^2 N(E_F)$, where μ_B is the Bohr magneton and $N(E_F)$ is the density of states at the Fermi level E_F, is considered. Thus χ_0 in equation (3) should contain χ_P:

$$\chi_0 = \chi_P + \chi_{orb} + \chi_{dia}. \quad (4)$$

For a strongly correlated metal system, it is known that the susceptibility has a significant temperature variation due to a large reduction of E_F or a large enhancement of the effective mass for the Pauli susceptibility. However, in the present case, the temperature region measured is limited below 300 K, so that the Pauli susceptibility may be nearly temperature independent [26]. Since the magnitude of $\chi_{orb} + \chi_{dia}$ is expected to be of the order of 10^{-5}emu mol^{-1} [8], χ_0 roughly corresponds to χ_P. Here, the Landau diamagnetism is a minor contribution. For CoO_2 (P3) and $Na_{0.09}CoO_2$, $N(E_F)$ values are 12 and 16 eV^{-1}, respectively. The value of CoO_2 (P3) is roughly sample independent, although CoO_2 (P3) #2 contains considerable amounts of impurities and/or lattice imperfections. According to the correlated band local-density approximation (LDA) for CoO_2 (O1), $N(E_F) \approx 4.5$ eV^{-1} [27], which leads to the effective mass of $m_{eff} \simeq 2.6\, m_0$ for CoO_2 (P3), m_0 being the free electron mass.

The ESR spectra for $Na_{0.09}CoO_2$ are approximately expressed by a Lorentzian. The temperature dependences of g and the peak-to-peak linewidths W of absorption derivatives are shown in figure 6. As the temperature is lowered, the g-factors vary from 2.35 to 2.25 between 250 and 140 K, below which they are almost constant down to 30 K. The linewidths decrease above 80 K, below which they are approximately constant down to 30 K. At $T_c \simeq 28$ K, g and W both increase rapidly. The result of $g \approx 2.3$ indicates that magnetically active ions correspond to Co^{4+}, having one hole in the dϵ shell for a strong octahedral field [28]. Unfortunately, the present specimens are powder and the linewidths are significantly large, so that precise determinations of the g anisotropy and spin susceptibility are difficult. These ESR results are a little similar to those of Na_xCoO_2 with $0.65 \leqslant x \leqslant 0.75$ [29] and they are in contrast with those for partially valence ordered phase $Na_{0.5}CoO_2$ [30].

It is known that some low-dimensional antiferromagnets lead to significant temperature variations of g due to a short-range ordered effect [31], but this is not the case, since this compound seems to exhibit a Pauli paramagnetism. Note that the soft-chemistry synthesis often gives rise to stacking faults as in the case of CoO_2 (P3). Moreover, the present compound has a structural disorder for partially occupied Na ions. In Co^{4+} for a strong octahedral field, even the slight difference of the ground state wavefunctions is known to give a significant

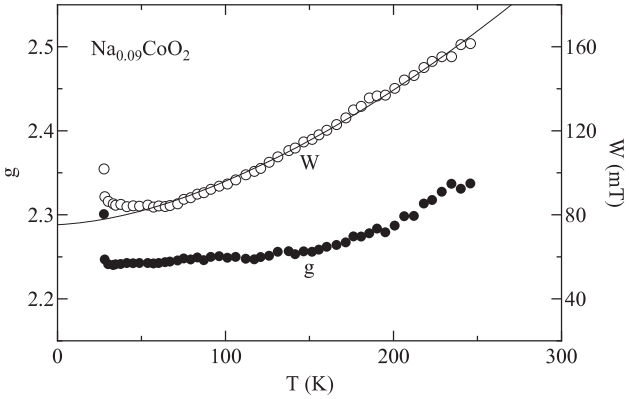

Figure 6. The temperature dependences of the ESR g-factor and the peak-to-peak linewidths of absorption derivatives for $Na_{0.09}CoO_2$, where the full curve provides the power of $r \approx 1.6$.

change of g [28]. Thus, the ordering of structural disorder probably leads to the change of g. One of the possible causes for a significant temperature variation of the linewidths may be the spin–lattice relaxation based on the Elliott mechanism [32], in which the relaxation rate or ESR linewidth is proportional to the scattering rate τ^{-1} and the square of g shift $|\Delta g|^2$. Considering that the intrinsic temperature dependence of the resistivity is given by T^2, the linewidth at high temperatures should be proportional to T^2 at high temperatures and become constant at low temperatures except for the effect of $|\Delta g|^2$. Assuming that the temperature dependence of the linewidth has the form $W = W_0 + CT^r$, where W_0 is a constant linewidth, one obtains $r \approx 1.6$ above 40 K as shown by the full curve in figure 6, which seems to be consistent with the Elliott model. The anomaly at $T_c \simeq 28$ K may not be of magnetic origin but may have the structural cause described above, since the magnetic susceptibility does not show a significant anomaly.

4. Conclusions

A chemical extraction of Li from $LiCoO_2$ with H_2SO_4 is confirmed to provide CoO_2 (P3) with a three-layer structure, as pointed out previously [11]. Using x-ray powder diffraction, ICP, TG, and MAS NMR, the structure is approximately modelled by the triangular lattice $Co^{4+}O_2$ with a prismatic oxygen environment between the layers. Here the oxygen concentration is close to the stoichiometric value. This structure has light stacking faults with shift vectors $\boldsymbol{s}_1 = \frac{2}{3}\boldsymbol{a} + \frac{1}{3}\boldsymbol{b}$ and $\boldsymbol{s}_2 = \frac{1}{3}\boldsymbol{a} + \frac{2}{3}\boldsymbol{b}$ along the shift of $\frac{1}{3}\boldsymbol{c}$. Such a structural aspect sometimes appears in layered transition-metal oxides synthesized soft-chemically [33].

CoO_2 (P3) is a weakly correlated metal on the basis of results for the thermoelectric power and the magnetic susceptibility, as in the case of $H_{0.3}CoO_2$ [8]. On the other hand, the electrical resistivity apparently shows a nonmetallic behaviour, but this may be explained with a parallel combination of the Fermi-liquid transport and the VRH transport in three dimensions due to the loose packing of specimens. The mass enhancement of CoO_2 (P3) with negligible Stoner factor is $m_{eff}/m_0 \approx 2.6$, which is smaller

than the value for $H_{0.3}CoO_2$, $m_{\rm eff}/m_0 \approx 5$ obtained using $N(E_{\rm F}) \approx 2$ eV^{-1} for $Na_{1/3}CoO_2$ [8]. Taking account of this reduction of Fermi energy and the result of thermoelectric power, the energy dependence of conductivity is considered to have the form $\sigma(E) \propto E^{0.2}$. On the other hand, if the ratio of correlation energy to bandwidth for CoO_2 (P3) and $H_{0.3}CoO_2$ is not so different, the Pauli susceptibility of CoO_2 (P3) should be about 1.14 times larger than that of $H_{0.3}CoO_2$, assuming $N(E_{\rm F})$ in three dimensions. This is a little smaller than the ratio of χ_P for CoO_2 (P3) to that for $H_{0.3}CoO_2$, about 1.3, which suggests that the electron correlation increases slightly as the carrier number approaches unity. A definite conclusion will be obtained through the correlated band LDA for $H_{0.3}CoO_2$.

$Na_{0.09}CoO_2$ also exhibits metallic properties. The Pauli susceptibility of this compound is significantly larger than those of CoO_2 (P3) and $H_{0.3}CoO_2$, which may be attributed to the difference in mass enhancement and/or $N(E_{\rm F})$. The ESR measurements provide a g-factor of 2.3 for Co^{4+} in a strong octahedral field. For a further understanding of the electronic state, a detailed structural study is necessary.

Acknowledgment

The authors thank Y Kikuchi for his help with the experiments in the early stage of this work.

References

[1] See, for example, Imada M, Fujimori A and Tokura Y 1998 *Rev. Mod. Phys.* **70** 1039
[2] Terasaki I, Sasago Y and Uchinokura K 1997 *Phys. Rev.* B **56** R12685
[3] See, for a recent topic Onoda M and Onoda M 2006 *Phys. Rev.* B **73** 104108
[4] Takada K, Sakurai H, Takayama-Muromachi E, Izumi F, Dilanian R A and Sasaki T 2003 *Nature* **422** 53
[5] Fouassier C, Matejka G, Reau J-M and Hagenmuller P 1973 *J. Solid State Chem.* **6** 532
[6] Onoda M and Ikeda T 2007 *J. Phys.: Condens. Matter* **19** 186213 and references therein
[7] Foo M L, Wang Y, Watauchi S, Zandbergen H W, He T, Cava R J and Ong N P 2004 *Phys. Rev. Lett.* **92** 247001
[8] Onoda M and Kikuchi Y 2007 *J. Phys.: Condens. Matter* **19** 346206
[9] See, for example, Antolini E 2004 *Solid State Ion.* **170** 159 and references therein
[10] Amatucci G G, Tarascon J M and Klein L C 1996 *J. Electrochem. Soc.* **143** 1114
[11] Venkatraman S and Manthiram A 2002 *Chem. Mater.* **14** 3907
[12] de Vaulx C, Julien M-H, Berthier C, Hébert S, Pralong V and Maignan A 2007 *Phys. Rev. Lett.* **98** 246402
[13] Ikeda T and Onoda M 2006 *J. Phys.: Condens. Matter* **18** 8673
[14] Altomare A, Burla M C, Camalli M, Carrozzini B, Cascarano G, Giacovazzo C, Guagliardi A, Moliterni A G G, Polidori G and Rizzi R 1999 *J. Appl. Crystallogr.* **32** 339
[15] Petricek V, Dusek M and Palatinus L 2000 *Jana2000* The Crystallographic Computing System Institute of Physics, Praha, Czech Republic
[16] Shannon R D 1976 *Acta Crystallogr.* A **32** 751
[17] See, for review, Onoda M and Nagasawa H 1994 *Butsuri (Bull. Phys. Soc. Japan)* **49** 559 (in Japanese)
[18] Brese N E and O'Keeffe M 1991 *Acta Crystallogr.* B **47** 192
[19] Treacy M M J, Newsam J M and Deem M W 1991 *Proc. R. Soc.* A **433** 499
[20] Brenig W, Döhler G H and Heyszenau H 1973 *Phil. Mag.* **27** 1093
[21] Onoda M and Yasumoto M 1997 *J. Phys.: Condens. Matter* **9** 5623
[22] Onoda M and Kohno M 1998 *J. Phys.: Condens. Matter* **10** 1003
[23] Beni G and Coll C F III 1975 *Phys. Rev.* B **11** 573
[24] Onoda M, Kikuchi Y and Sugawara A 2007 *Meet. Abstr. Phys. Soc. Japan* **62** (2) 638
[25] See, for example, Ashcroft N W and Mermin N D 1976 *Solid State Physics* (Philadelphia, PA: Saunders College)
[26] See, for example, Wilson A H 1958 *The Theory of Metals* 2nd edn (London: Cambridge University Press)
[27] Lee K-W and Pickett W E 2005 *Phys. Rev.* B **72** 115110
[28] Abragam A and Bleaney B 1970 *Electron Paramagnetic Resonance of Transition Ions* (Oxford: Clarendon)
[29] Carretta P, Mariani M, Azzoni C B, Mozzati M C, Bradarić I, Savić I, Feher A and Sebek J 2004 *Phys. Rev.* B **70** 024409
[30] Sakurai T, Takano S, Ohta H, Sakurai H and Takayama-Muromachi E 2007 *J. Magn. Magn. Mater.* **310** e275
[31] Oshikawa M and Affleck I 2002 *Phys. Rev.* B **65** 134410 and references therein
[32] Elliott R J 1954 *Phys. Rev.* **96** 266
[33] See, for example, Onoda M, Wang L, Takada K and Sasaki T 2007 *Phil. Mag.* **87** 2767